Impact of ionizing radiation on iodine capture by functionalized mesoporous silica

C. Rey, G. Zante, J. Causse, X. Deschanels, S. Le Caër

Impact of ionizing radiation on iodine capture by functionalized mesoporous silica

C. Rey,[a] G. Zante,[b] J. Causse,[a] X. Deschanels[a] and S. Le Caër[b*]

[a] *ICSM, Université de Montpellier, CEA, CNRS, ENSCM, Bagnols-sur-Cèze 30200, France*

[b] *Université Paris-Saclay, CEA, CNRS, NIMBE, UMR 3685, 91191, Gif-sur-Yvette, France*

*Corresponding author

E-mail address: sophie.le-caer@cea.fr

Abstract

The efficient capture of radioactive iodine is an important challenge for the nuclear industry, in order to prevent risks for the environment and for the health. The use of solid sorbent materials, able to capture significant amounts of iodine and to resist to harsh operating conditions, such as radiation, is then of paramount interest. Here, we have grafted a high surface area mesoporous silica, SBA-15, with the N-[3-(trimethoxysilyl)propyl]ethylenediamine "diamino" ligand. The resulting material is able to capture significant amounts of iodine (around 0.23 g per gram of material) due to a strong interaction between iodine and the lone pairs of the nitrogen atoms. We have also investigated the behavior of this grafted material towards ionizing radiation in order to assess its stability when placed in a radioactive environment. Upon irradiation, radiolysis of the ligand led to H_2 production due to preferential cleavage of the N-H bonds, rather than cleavage of C-H bonds, hence forming imine functional groups as evidenced by infrared spectroscopy. After irradiation at the dose of 1 MGy, the thus-modified materials were still able to capture iodine, but in a lower proportion (around 0.11 g per gram of material). This was attributed to the loss of amine groups upon irradiation. Our work shows that these materials are potential candidates for the radioactive iodine capture, as they can be efficient up to doses of the order of 1 MGy.

Keywords

Grafted mesoporous silica, iodine capture, radiolysis, reaction mechanisms

1. Introduction

Radioactive iodine is produced by fission reactions in nuclear reactors. It is a β^- emitter having a long-lived isotope ^{129}I ($T_{1/2} = 1.6\times10^7$ years) and a short-lived one ^{131}I ($T_{1/2} = 8$ days) (Hou et al., 2009; García-Toraño et al., 2018). During normal reactor and fuel reprocessing operations, a very small fraction of the radioactive elements present is found in the effluents discharged into the environment. Among the effluents released, radioactive iodine can for instance be in the form of gaseous molecular diiodine (I_2). As radioactive iodine is dangerous for health (especially ^{131}I) and volatile, one important goal of nuclear industry is to capture it efficiently and selectively during fuel reprocessing. Of course, ^{129}I is also of great concern due to its long half-life. Therefore, it has to be safely stored on the geological timescale (Simpson, 2013; Riley et al., 2016).

To reach this goal, many different aqueous scrubbings (either acidic or basic) have been tested. However, these techniques imply various steps as well as the formation or use of dangerous chemical species. Therefore, solid sorbents are appealing for the immobilization of radioactive iodine. For instance, silver exchanged zeolites, among other possible materials, are currently used in nuclear plants, the capture of iodine leading to the formation of AgI (Chapman et al., 2010; Maddrell et al., 2015; Sava Gallis et al., 2017). However, this process is expensive, and other porous solids were explored (Huve et al., 2018): various metal-organic frameworks (MOFs) able to capture iodine from vapor or solvent (Valizadeh et al., 2018; Tang et al., 2019; Chen et al., 2020), titanosilicates (Nandanwar et al., 2016), Hofmann clathrates (Massasso et al., 2015), porous organic polymers (Chen et al., 2015; Qian et al., 2016; Zhu et al., 2017).

Among the various possible porous solids, mesoporous silica retains our attention. Indeed, they have attracted much interest in the nuclear community as possible storage media for various radioactive materials (Sangvanich et al., 2010; Makowski et al., 2012). A large volume of ordered mesopores gives these silicas a high surface to volume ratio while their easily modifiable surfaces, and their resistance to acidic and radioactive environments, makes them excellent candidates for the extraction and subsequent trapping of various radionuclides. Moreover, these materials can be further modified with specific radionuclides binding sites allowing them to chemically separate, trap and retain target species from solution. Therefore,

modified mesoporous silica was already used for the capture of radioactive iodine (Mnasri et al., 2014; Massasso et al., 2015; Yang et al., 2015). However, all the modified mesoporous silicas cited just above contain metallic elements such as Bi, Ni, Ag. However, it is possible to modify mesoporous silica with organic functional groups, thus avoiding the use of metals that may be expensive or scarce. Among the various functional groups able to capture iodine, amines, and especially diamine functional groups, are particularly appealing due to the interaction between iodine and the σ-electron donor nitrogen atoms (Massasso et al., 2015). Once functionalized, mesoporous silica can be used as a "sponge" removing and trapping the species as the active solution passes through. When the mesoporous silica is full with radioactive species, it can then be vitrified (Lago et al., 2022). Alternatively, the silica mesoporosity could be closed under relatively mild conditions by the application of mechanical stress or even radiation damage (Lou et al., 2017; Lin et al., 2021). For these organically-modified inorganic materials to be viable alternatives to today's industry standards, they must remain stable under ionizing radiation. While the silica moiety is inorganic and therefore relatively stable upon irradiation, the organic grafting moiety should be more sensitive towards ionizing radiation. However, the radiolytic stability of these materials is not assessed in literature. This is nevertheless very important as one has to make sure that iodine does not escape from the silica matrix before vitrification.

We chose to work with SBA-15 as a typical mesoporous silica in the present study. Indeed, SBA-15 was found to be more robust towards irradiation than another mesoporous silica, MCM-41.(Lou et al., 2015) It was then grafted with a ligand containing a diamine functional groups, i.e. N-[3-(trimethoxysilyl)propyl]ethylenediamine. After synthesis of the material, the aim of the present work was the following: i) understand in details the behavior of this material under accelerated electrons irradiation. Indeed, they can mimic the behavior of a β^- emitter such as ^{129}I and ^{131}I; ii) assess the sorption ability of this material towards iodine; iii) determine the influence of irradiation on iodine sorption. The goal is to describe reaction mechanisms at stake in these grafted materials under irradiation, and to understand how this can affect the iodine capture properties.

2. Materials and methods

2.1. Synthesis of materials

Chemicals. All chemicals were purchased from commercially available sources and used as received. Tetraethylorthosilicate (TEOS), Pluronic 123 (P123), N-[3-(trimethoxysilyl)propyl]ethylenediamine (Diamino), dry toluene and diiodine were purchased from Sigma Aldrich. HCl and cyclohexane were purchased from Alfa Aesar.

Synthesis of SBA-15. SBA-15 was prepared according to literature protocol of Zhao et al. (Zhao et al., 1998). The final molar ratio TEOS/P123/HCl/H_2O was 1: 0.017: 6: 144. The material obtained was labelled as SBA-15.

Synthesis of functionalized SBA-15. In a typical recipe, 2.00 g of SBA-15 was heated at 90°C under vacuum for 24 hours in order to activate the –OH groups on the surface. Then 50 mL of dry toluene was added under argon. After stirring for 10 min, 4.432 g of N-[3-(trimethoxysilyl)propyl]ethylenediamine was added to the solution and reflux conditions were set at 95°C for 24 hours. The materials were subsequently filtrated with ether and dried at ambient temperature for 24 hours. The SBA-15 grafted with the diamino ligand was labelled as SBA-15-D (see Scheme 1).

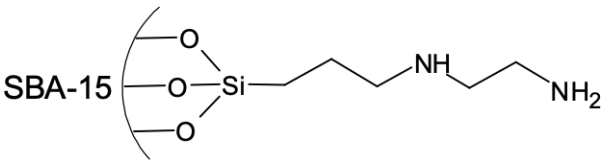

Scheme 1. *Structure of SBA-15-D*

Iodine capture. A solution of diiodine in cyclohexane at a concentration ranging between 0 and 3.1 x 10^{-3} M was added to a few hundred mgs of SBA-15-D, or to 5 mg of SBA-15-D-1MGy (corresponding to the grafted silica irradiated at 1 MGy, with 1 Gy = 1 $J.kg^{-1}$), and the mixture was stirred for 24 hours at room temperature under air. Experiments were performed with a powder-solution ratio of 1 $mg.mL^{-1}$. The resulting material was then placed in a cartridge in a Soxhlet apparatus and thoroughly washed with cyclohexane for 24 hours in order to eliminate iodine that could be sorbed via a weak interaction on sites other than the di-amino graft. The iodine content within the material was determined by measuring the residual concentration of diiodine in solution by UV-Visible spectroscopy. The SBA-15-D material after iodine capture was labelled as SBA-15-D-I_2.

2.2. Characterization of materials

Thermogravimetric analysis (TGA). TGA experiments coupled to mass spectrometry **(**TGA-MS) analyses were performed with a Setaram Setsys Evolution 16 Instrument in an alumina crucible of 100 µL. The mass spectrometer was a Hiden QGA300 Instrument allowing performing gas analysis. The thermal treatment of the samples ranged from 25 to 1000 °C, at a heating rate of 5 °C.min^{-1} and was performed under air with a flow rate of 20 mL.min^{-1} in order to quantify the organic decomposition of the ligand and, when present, of trapped iodine.

Elementary analysis. Carbon and nitrogen elementary analysis were performed on LECO CS230 and LECO TCH600 apparatus respectively.

Nitrogen adsorption/desorption analysis. These analyses were carried out at 77 K with a Micromeritics ASAP- 2020 instrument. Before each measurement, samples were outgassed (350°C for 4 hours for SBA-15 and 80°C for 48 hours for functionalized SBA-15). The specific surface and pore volume were calculated by using the BET (Brunauer, Emmett, Teller) method based on a multilayer adsorption model and the pores size distribution was calculated by the BJH (Barret, Joyner, Halenda) model on the desorption branch.

Small angle X-ray scattering (SAXS). SAXS experiments were performed by using a Guinier-Mering setup with a 2D image plate detector. The X-ray source consisted of molybdenum, which delivers a high-energy monochromatic beam (λ = 0.71 Å, E = 17.4 keV), providing structural information over scattering vectors *q* ranging from 0.2 to 30 nm^{-1}. Helium flowed between the sample and the image plate to prevent air adsorption. The sample acquisition time was 900 s. Data corrections and radial averaging were performed by standard procedures.

X-ray photoelectron spectroscopy. XPS was performed with a hemispheric analyzer Kratos Analytical Axis Ultra DLD spectrometer, using an Al Kα source monochromatized at 1486.6 eV and a charge compensation system. A pass energy of 160 eV was used for the survey spectra and of 20 eV for core levels measurements. The energy resolution of the source and of the analyzer was found to be 0.35 eV. A thin layer of the sample was deposited on a copper tape. In all cases, the carbon C 1s line at 284.8 eV was used as a reference to calibrate the binding energy. Data acquisition and processing were carried out using the Casa XPS processing software. After calibration, the background from each spectrum was subtracted using a Tougaard-type background.

Spectroscopic characterization (UV-Visible, Raman and infrared spectroscopy)

UV-Visible spectroscopy was performed on a Thermo Scientific Evolution 220 set-up in order to measure the residual concentration of diiodine in cyclohexane solution (see above). The equilibration time was about 30 s. The absorption band of diiodine in the solution had a maximum at 524 nm with a molar absorption coefficient of 1800 $mol^{-1}.L.cm^{-1}$.

Raman spectra were recorded on a Horiba Jobin Yvon LabRAM Aramis confocal Raman microscope was operated with an excitation wavelength of 532 nm, a laser spot size of 1 µm and an objective of 50x long working distance. The incident laser power was kept lower than 0.8 mW in order to avoid any heating or structural damage to the sample.

Infrared (IR) spectra were recorded using a Bruker Vertex 70 FT-IR apparatus. 1% (mass) of the sample was dispersed into KBr and compacted into pellets, and then placed in the apparatus. The spectra were recorded in the 370-5000 cm^{-1} range with a 4 cm^{-1} resolution and averaged from 100 scans. The KBr background was subtracted in all cases.

2.3. Irradiation experiments

Irradiation of the samples. For the irradiation experiments, around 300 mg of the sample was weighted using a Sartorius ED124S balance (precision ± 0.1 mg) and placed into a Pyrex glass ampoule. The sample was heated under vacuum at 140°C during 16 hours in order to remove residual water and organic contaminants. After the thermal treatment, the ampoule was outgassed and filled with 1.55 bar of argon. The operation was repeated three times before each irradiation to ensure that the atmosphere of the ampoule before irradiation was made of pure argon. Next, the sample was irradiated using a Titan Beta Inc. linear accelerator providing 10 ns pulses of 10 MeV electrons. The repetition rate was fixed at 5 Hz.

Fricke dosimetry was used to determine the dose received by the sample (Fricke,Hart, 1966). The dose received by the solution was estimated to be 15 Gy per pulse and was considered to be similar to the dose received by all mesoporous silica samples (Brodie-Linder et al., 2010).

SBA-15-D samples were irradiated at 1 MGy and then used to sorb iodine. They are then labelled as SBA-15-D-1MGy and SBA-15-D-1MGy-I_2, respectively. Samples having sorbed iodine were also irradiated in order to study the impact of irradiation on iodine fate. They are labelled as SBA-15-D-I_2-500kGy and SBA-15-D-I_2-2.5MGy, for irradiation doses of 500 kGy and 2.5 MGy, respectively.

Gas produced upon irradiation. After irradiation, H_2, CO, CO_2 and CH_4, if produced, were measured by micro-gas chromatography (μ-GC) using an SRA-instrument IGC-R3000 apparatus. The gases produced under irradiation were diluted to a total pressure of 1.5 bar with ultrapure argon (99.9999%) for 5 minutes prior to the analysis. These experiments were reproduced at least two times to ensure reproducibility. Results were found to be reproducible within a 10% error bar.

In order to assess the nature of the gases produced upon irradiation, complementary gas chromatography measurements coupled to mass spectrometry (GC-MS) were performed using an Agilent 7890 GC system associated to an Agilent 5977 MSD mass spectrometer with a quadrupole analyzer. Helium was used as a vector gas at a flow rate of 2 $mL.min^{-1}$. The separation was carried out in split mode with a PorabondQ (25 m × 0.32 mm) column (Agilent). Injector was set at 110°C. The mass ranged between 1 and 200 amu and the detection limits were around 1 ppm. GC-MS analysis was carried out at least two times for each sample.

3. Results and discussion

3.1. Characterization of the materials before and after grafting

The surface area, pore size and pore volume of the SBA-15 materials were investigated by N_2 adsorption-desorption measurements (Figure S1). The isotherms exhibit a H1 hysteresis loop that is characteristic of mesoporous solids such as SBA-15. Pristine SBA-15 has the highest specific surface (774 $m^2.g^{-1}$). As expected, a decrease of the specific surface to 235 $m^2.g^{-1}$ is observed after grafting of the organic compound (see Table 1) (Zante et al., 2022). This is assigned to the filling of the pores by grafting, as evidenced also by the decrease of the pore size (from 7.0 to 6.6 nm after grafting) and of the porous volume (from 1.17 to 0.49 $cm^3.g^{-1}$ after grafting). Notably, most of the grafted molecules are expected to be located within the porous structure of the silica since there is much less external surface area than internal area. On SAXS patterns (shown in Figure S2), five peaks were observed for all samples, which implies that the hexagonal p6mm symmetry of the mesoporous SBA-15 is maintained after grafting and iodine capture. However, a variation in the intensity of the peaks is observed, which reflects an evolution of the porous structure. These diagrams were fitted using the method described in reference (Cambedouzou,Diat, 2012), taking into account the layers of

diamino and iodine attached to the surface of the silicas. The results obtained did not make it possible to obtain a more precise description of the surface of the pores.

TGA-MS experiments were performed on SBA-15 and SBA-15-D samples (Figure S3a). Overall, these analyzes show that the thermolysis of the ligands grafted at the surface of the silica is complete at 650°C. For SBA15-D, the final mass loss at 650°C is equal to 35.5%. A first mass loss of about 11.5% is attributed to H_2O and CO_2. It is observed for temperatures lower than 130°C (see Figure S3b). The second mass loss is due to the thermolysis of the diamino ligand as evidenced by mass spectrometry which indicates the release of the gaseous species (H_2O, NO_2, CO_2, see Figure S3b). This mass loss is equal to 24.5% of the total mass (Table 1).

The results of the elementary analysis are presented in Table 1. The greater C/N ratio (for instance, C/N = 4.3 in SBA-15-D) than the expected one in the diamino group (C/N = 2.14) can be interpreted as the presence of CO_2 sorbed in the material. Indeed, amine-functionalized mesoporous silica is known to adsorb CO_2.(Serna-Guerrero et al., 2010) The final mass balance obtained by summing the percentages of the diamino groups and of CO_2 calculated from the C, N elemental analyzes is consistent with the TGA measurement (Table 1, with 23.3% vs 24.5% in the case of SBA-15-D).

Table 1. *Summary of the surface area (S_{BET}), porous volume (Vp) and pore diameter (Dp) of the various materials under study. Elementary analyses (%C and %N) were used to calculate the percentages of CO_2 and diamino groups. Indeed, as the C/N ratio in the samples is greater than the theoretical ratio 2.14 for diamino ligand, it is assumed that there is CO_2 in the samples. The mass loss (Δm) was obtained from TGA measurements (Figure S3). It was performed between 130°C and 650°C in order to remove adsorbed water contribution (Figure S3). Δm could not be measured in the case of the SBA-15-D-1MGy-I_2 sample due to a too low amount of sample available. In the case of SBA-15-D-I_2, the difference between Δm and % ligand indicates that roughly 28.4% of the sample is iodine.*

Sample	**S_{BET} ($m^2.g^{-1}$)**	**Vp ($cm^3.g^{-1}$)**	**Dp (nm)**	%C wt	%N wt	% diamino (wt%)	% CO_2 (wt%)	% (CO_2 + diamino) (wt%)	% Δm (TGA) (wt%)
SBA-15	774	1.17	7.0	0.14	0.003	-	-	-	-
SBA-15-D	235	0.49	6.6	13.8	3.2	11.6	11.7	23.3	24.5
SBA-15-D-I_2	100	0.18	6.5	10.1	2.9	10.5	6.6	17.1	45.5

SBA-15-D-1MGy-I_2	31	0.05	5.7	12.4	2.5	9.0	11.9	20.9	-

The grafting density of the diamino group ρ (expressed in groups·nm^{-2}) in SBA-15-D was calculated based on the nitrogen content in the sample according to Eq. 1:

$$\rho = \frac{\%N \times N_A}{M^N_{grafted}} \frac{10^{-18}}{(100-\%N)\, S_{BET}} \quad \text{(Eq. 1)}$$

where (%N) is the nitrogen percent of the sample, N_A is Avogadro's constant, $M^N_{grafted}$ is the N molecular weight in the grafted group (28 g.mol^{-1}) and S_{BET} is the specific surface area of SBA-15 before grafting (m².g^{-1}). A grafting density of 0.92 groups.nm^{-2} was obtained, which is consistent with the values generally found in grafted mesoporous silicas (Sanchez-Vicente et al., 2020). Knowing that there are roughly 6 –OH groups.nm^{-2} (Zhuravlev, 2000), then about one in six sites is grafted.

The grafting of the ligand was further confirmed thanks to spectroscopic experiments (XPS and FT-IR spectroscopy). Indeed, no intensity was observed on the N1s core-level spectrum of pristine SBA-15, while the presence of a band in the grafted SBA-15-D sample evidenced the presence of nitrogen atoms in the latter sample (Figure S4).

The incorporation of di-amino ligand within the SBA-15 matrix was also confirmed by infrared spectroscopy. The FT-IR spectrum is shown in Figure 1, while the assignment of the bands is provided in Table 2. Clearly, the spectrum of SBA-15-D is strongly modified as compared to that of SBA-15. Besides the bands characteristic of the silica matrix (such as the O-Si-O bending mode at 461 cm^{-1} or the broad Si-O asymmetric stretching mode between 1000-1200 cm^{-1}) other bands are found, which are characteristic features of –CH_2- groups and of amino functional groups. After grafting, isolated silanols are detected on the surface at 3749 cm^{-1}. The grafting of the ligand is evidenced thanks to the presence of vibrational groups typical of –NH_2 and –CH_2 modes (Figure 1 and Table 2). The presence of the secondary amine is more subtle to detect, as the corresponding vibrational modes are rather weak. Noteworthily, the C-N stretching vibration is usually detected in the 1000-1200 cm^{-1} wavenumber range (Meléndez-Ortiz et al., 2014), but these bands are masked by the strong bands of silica in this wavenumber range. However, the bands get broader after grafting in

this wavenumber range, suggesting that C-N modes overlap with those arising from silica. Lastly, the strong absorption detected between 2800 and 3200 cm^{-1} in SBA-15-D suggests that a part of $–NH_2$ groups, after interaction with surface silanol groups, gets protonated to form a primary amine salt $–NH_3^+$. Moreover, some weak features detected around 1550 and 1607 cm^{-1} also suggest the formation of these amine salts (Maria Chong,Zhao, 2003). Indeed, the presence of residual adsorbed water molecules or of acidic silanol groups was shown to promote proton transfer reactions from silanol groups to amino ones, leading to the formation of ammonium salts (Golub et al., 1996; Hijazi et al., 2019).

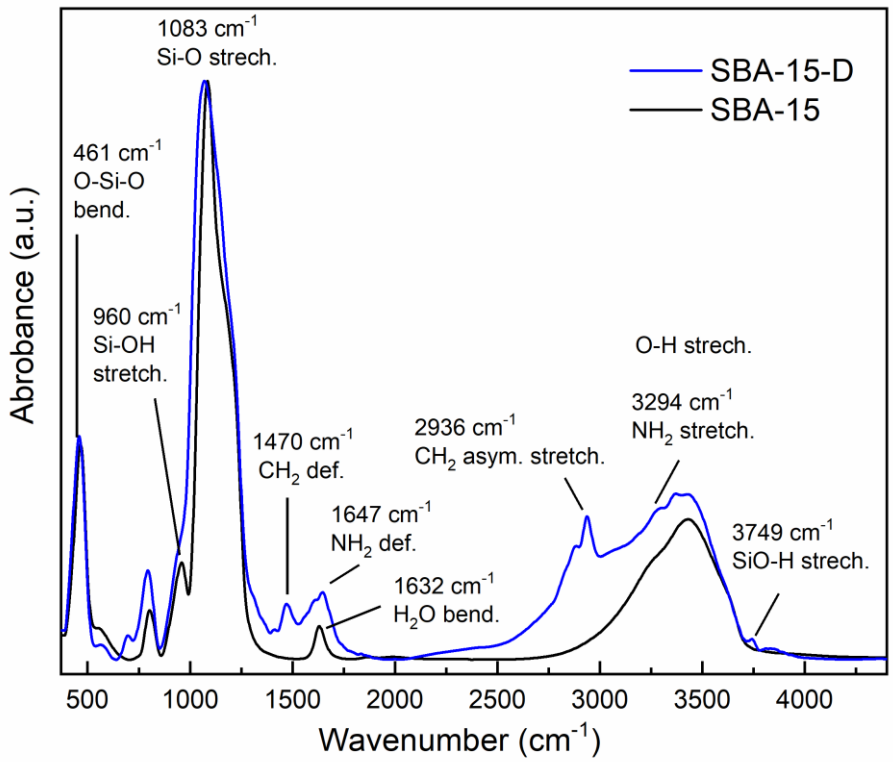

Figure 1. *FT-IR spectra of SBA-15 (black) and SBA-15-D (blue) after the thermal treatment. The spectra are normalized with respect to the Si-O stretching mode at 1083 cm^{-1}. The main bands of interest are indicated. Stretch. stands for stretching, bend. for bending and def. for deformation.*

Table 2. *Proposed assignment of the IR vibrational bands based on literature data (Colthup et al., 1990; Le Caër et al., 2005).*

Wavenumber (cm^{-1})	Assignment
461	O-Si-O bending

695	NH wagging
796	Si-O symmetric stretching
960	Si-OH stretch
1000-1200	asymmetric Si-O stretching
1470	CH_2 deformation
1550	$-NH_3^+$ symmetric deformation
1564	$-NH_2$ scissoring
1607	$-NH_3^+$ asymmetric deformation
1647	NH_2 deformation
1632	H_2O bending mode of adsorbed water molecules
1651	NH_2 deformation
2879 and 2936	CH_2 symmetric and asymmetric stretching, respectively
3000-3700	O-H stretching modes (from H-bonded SiO-H and adsorbed water molecules)
3300-3500	weak N-H stretching band
3294 and 3367	Symmetric and asymmetric NH_2 stretch, respectively
3749	O-H from isolated SiO-H groups

3.2. Behavior of SBA-15-D under irradiation

3.2.1. Gas production under irradiation

The gases produced upon irradiation in the pristine and grafted SBA-15 samples were measured by micro-gas chromatography. In both samples, the only gases detected by this technique were H_2 and CO_2. The evolution of the production of these gases as a function of the dose is depicted in Figure 2.

The H_2 production evolves linearly with the dose in both samples (Figure 2a), while the CO_2 production evolves slightly less linearly. Indeed, the CO_2 production is low and close to the detection limit of the set-up under our experimental conditions. Noteworthily, the samples are placed under vacuum during the preparation of the ampoules before irradiation. Therefore, sorbed CO_2 in SBA-15-D is released at this stage. This explains why the initial presence of sorbed CO_2 in the grafted material does not have any effect on the CO_2 production upon

irradiation. From the slopes of the lines, the various gas radiolytic yields, i.e. the amount of gas produced per energy deposited in the matter, are obtained. The H_2 radiolytic yield is equal to 0.14 ± 0.01 µmol.J^{-1} in the grafted sample. Obviously, it is higher than the yield measured in SBA-15 (0.08 ± 0.01 µmol.J^{-1}), and also higher than the value measured in bulk water (0.045 ± 0.04 µmol.J^{-1}) (Spinks,Woods, 1990). The H_2 radiolytic yield measured in the grafted sample is consistent, although higher, with measurements performed on other grafted SBA-15 samples (Zante et al., 2022). In this latter case, the major gas produced under irradiation was CO (and not H_2) due to the preferential radiolysis of the amide functional group.

Obviously, the H_2 production prevails, with a H_2 radiolytic yield ~ 50 times higher than the CO_2 one. Noteworthily, considering the error bars, the non-grafted and grafted materials have the same CO_2 radiolytic yield (0.002 µmol.J^{-1}). Since the CO_2 production is low and not affected by grafting, it can be attributed to the radiolysis of residual ethoxy groups present within the SBA-15 and SBA-15-D material (Maria Chong,Zhao, 2003).

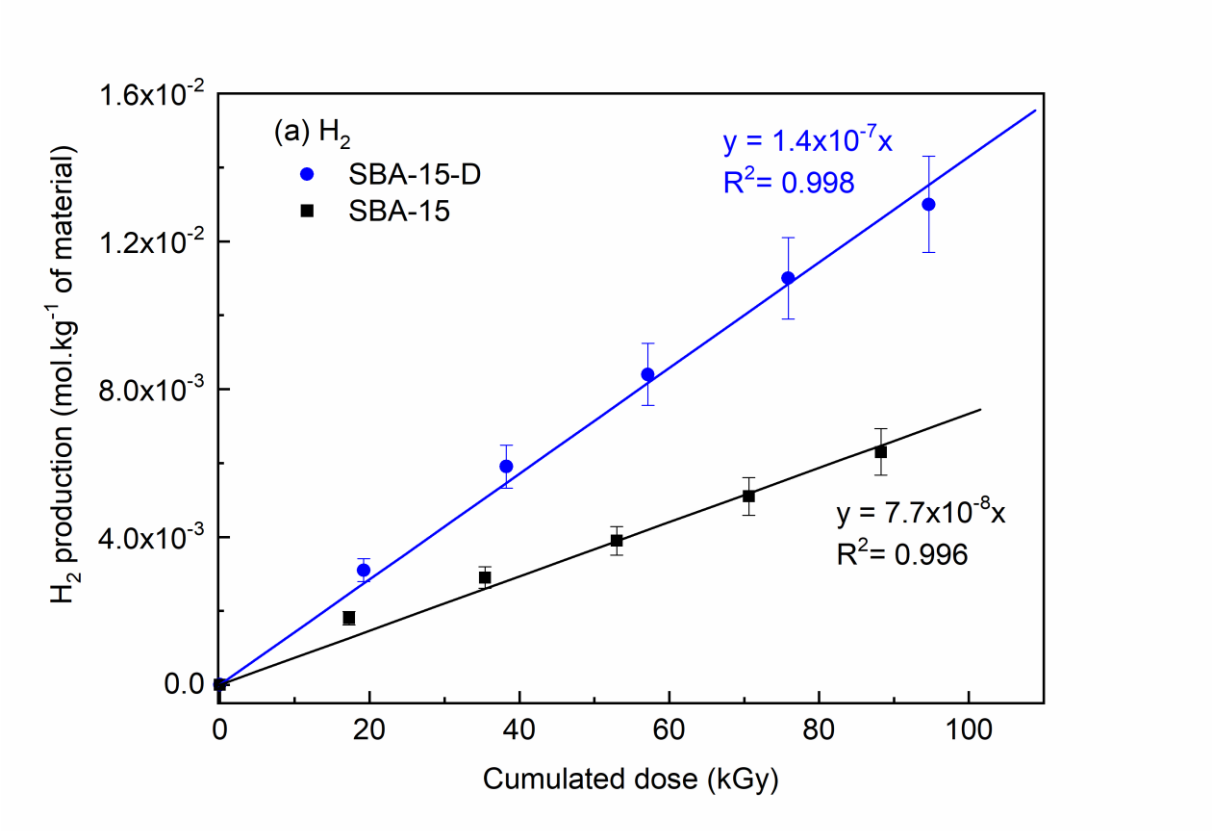

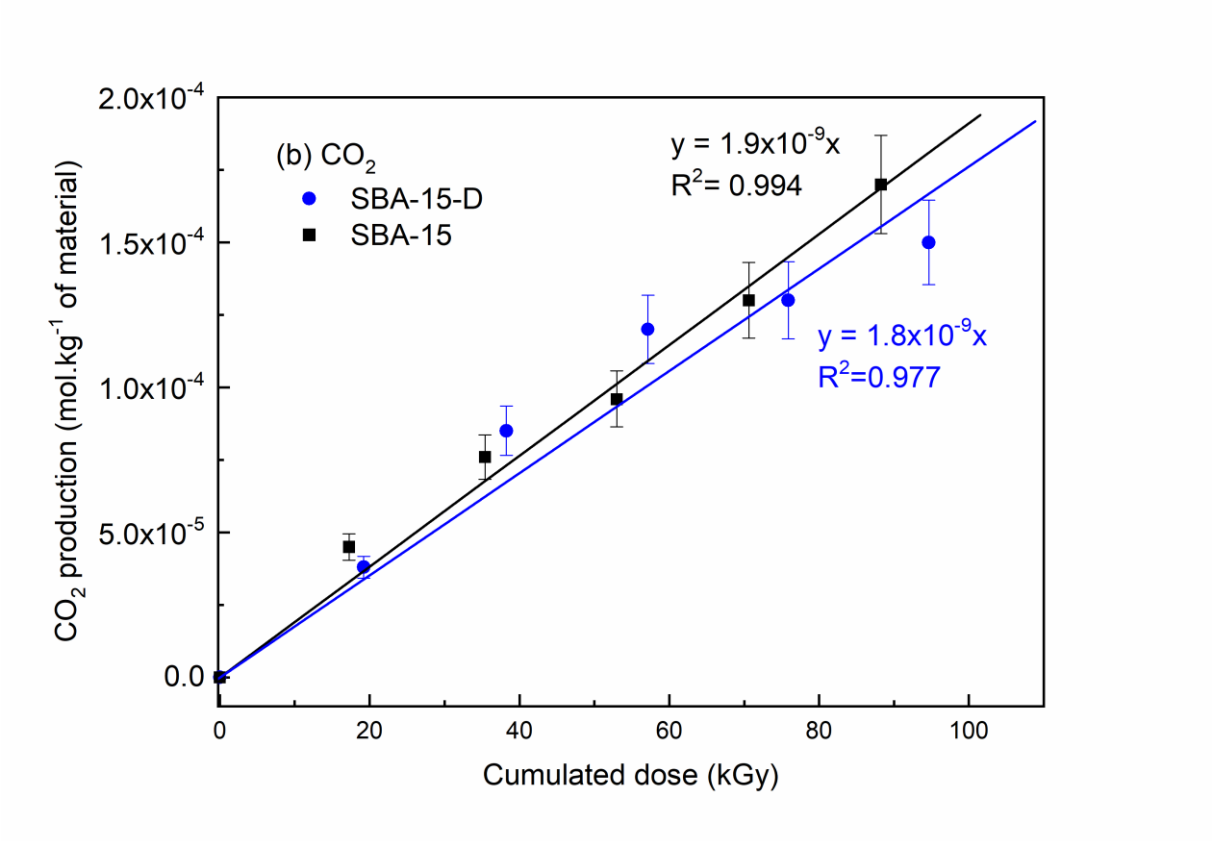

Figure 2. *(a) Evolution of the H_2 and (b) CO_2 production as a function of the cumulated dose (kGy). Each curve was fitted by a straight line, and the slope of the line, corresponding to the gas production radiolytic yield, expressed in mol.J^{-1}, is provided.*

GC-MS experiments were also performed in order to identify other gases that could be formed under ionizing radiation. After irradiation at 100 kGy, only one gas, carbon dioxide, was detected, both in SBA-15 and in SBA-15-D (figure S5). No other gases, such as alkanes, could be evidenced in irradiated SBA-15-D, showing that C-C bond cleavages are not likely to occur during the irradiation of SBA-15-D up to 100 kGy. The detection of amines or of ammonia can be difficult (Kataoka, 1996), therefore at this stage it is impossible to exclude their formation based on our experiments.

Clearly, the H_2 radiolytic yield increases in the grafted sample as compared to the pristine one. Radiolysis is known to affect physisorbed water molecules within the structure of SBA-15 (Brodie-Linder et al., 2010), by breaking the O-H bonds of water molecules eventually remaining within the material. Similarly, the rupture of O-H bonds from the silanols is another source of H_2 production for both SBA-15 and SBA-15-D samples. This accounts for the H_2 production in the pristine sample. Besides, the additional cleavage of C-H and N-H

bonds in the grafted ligand can account for the higher H_2 radiolytic yield measured in the grafted SBA-15-D as compared to the pristine one.

In order to understand more precisely the modifications of the SBA-15-D sample after irradiation, FT-IR experiments of this sample before and after irradiation were performed. The corresponding results are discussed below.

3.2.2. Behavior of SBA-15-D under irradiation

The FT-IR spectra of SBA-15-D before and after irradiation at 0.1 MGy and 1 MGy are given in Figure 3a, with a focus on spectral regions of interest in Figures 3b-3c.

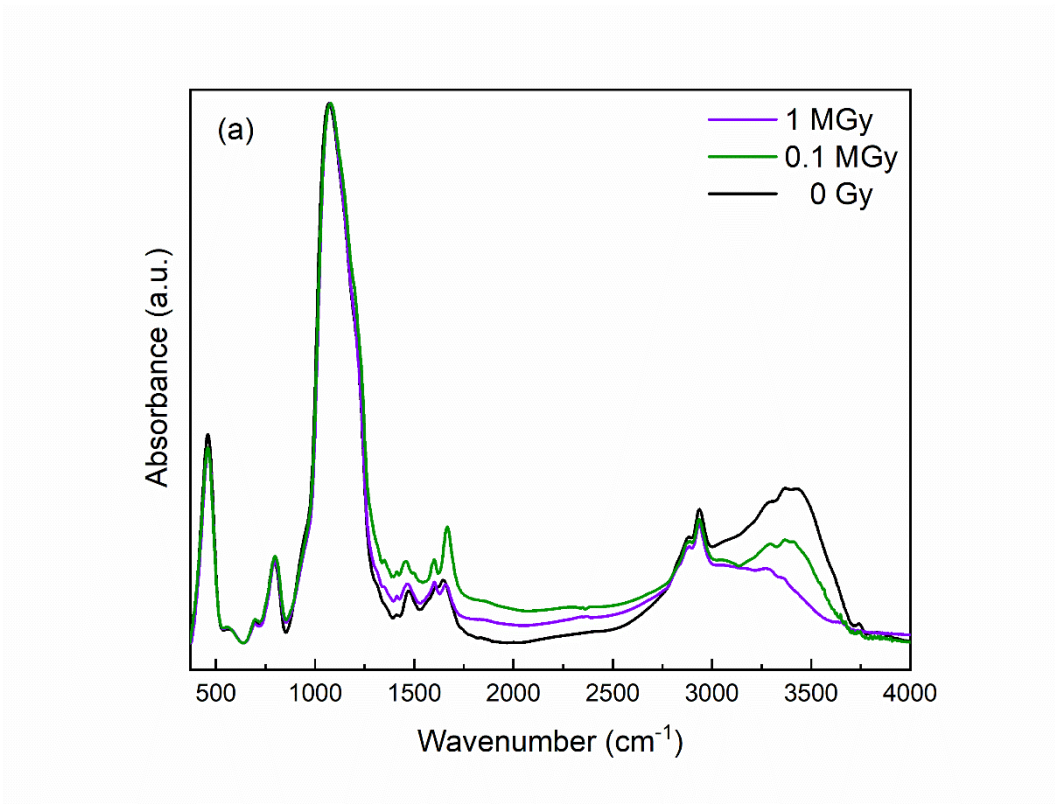

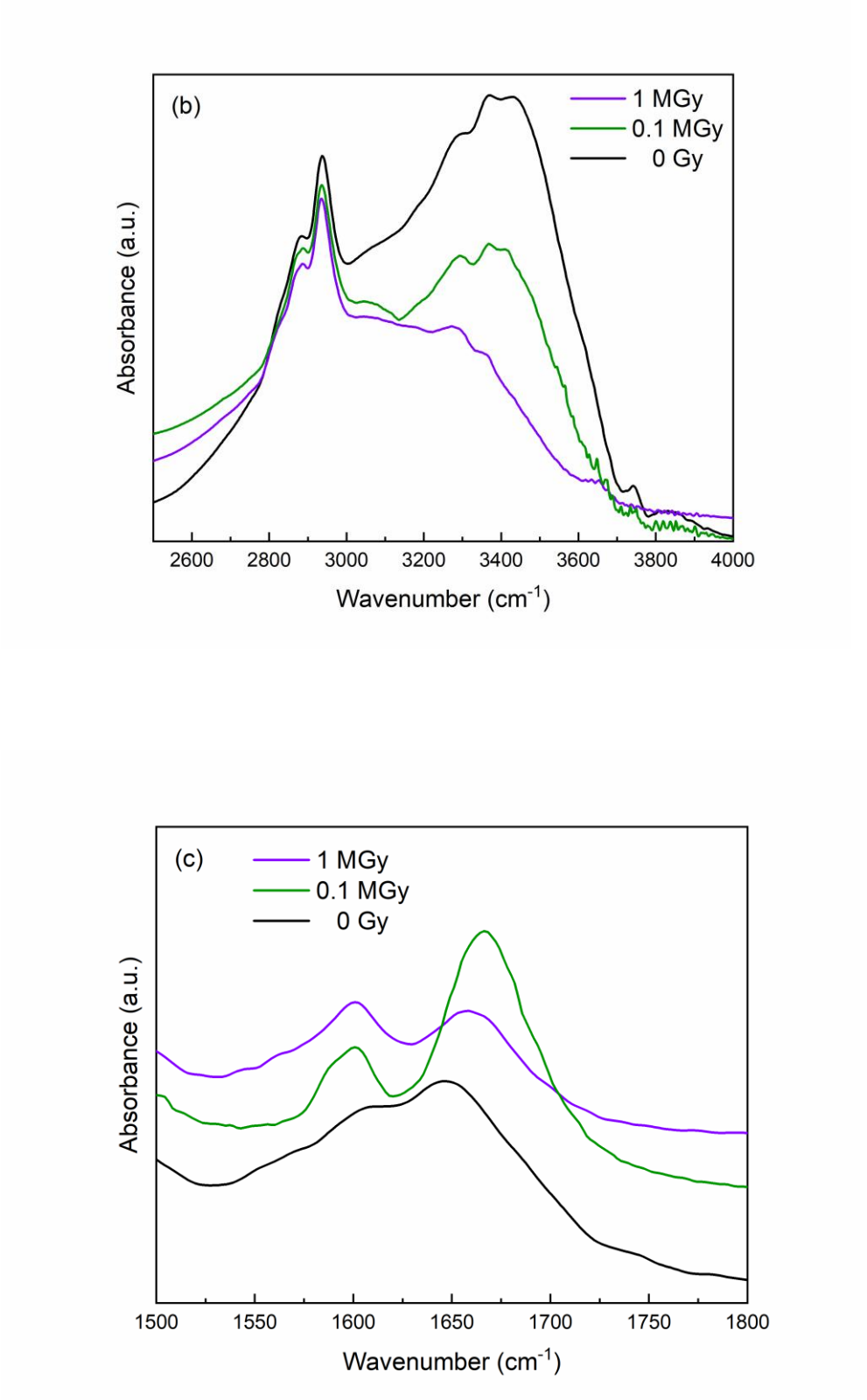

Figure 3. *(a) FT-IR spectra of SBA-15-D before (black) and after irradiation at 0.1 MGy (green) and 1 MGy (purple), and enlarged view in the (b) 2500-4000 cm^{-1} wavenumber range and (c) 1500-1800 cm^{-1} wavenumber range. In this latter case, the curves were offset for the sake of clarity. The spectra are normalized with respect to the Si-O stretching mode at 1083 cm^{-1}.*

Obviously from Figure 3, the characteristic bands of the SBA-15 matrix are not affected by irradiation. A striking difference between SBA-15-D before and after a 100 kGy irradiation arises from the O-H stretching band. Its intensity decreases upon irradiation. Clearly, silanols and adsorbed water molecules, if present, are affected by irradiation, even at the lowest irradiation dose. This effect is analogous to that of the thermal treatment.

Concerning the modification of the environment around the nitrogen atom, the band located at 1647 cm^{-1} is shifted towards 1667 cm^{-1} in the case of the sample irradiated at 100 kGy (Figure 3c). This band can be attributed to the formation of an imine (C=N bond in R_1-CH=N-R_2-type compounds (Colthup et al., 1990)). This suggests the formation of the C=N double bond mainly around the secondary amine of the grafted ligand.

When the irradiation dose increases to 1 MGy, the intensity of the $–CH_2$ groups also decreases (see the bands at 1468 cm^{-1} and around 2900 cm^{-1}, Figure 3), indicating that they are affected by irradiation. However, these modifications are modest as compared to the changes around the nitrogen atom (Figure 3b). This indicates that N-H bond are preferentially cleft as compared to C-H ones. This observation is consistent with the findings of a study on the radiolysis of quaternary ammonium salts (Dhiman,LaVerne, 2013). At this high dose, a strong decrease of the infrared intensity measured between 2800 and 3400 cm^{-1} indicates that -NH_2 and -NH_3^+ functional groups are strongly affected by ionizing radiation. In the 1600-1700 cm^{-1} spectral region, the maximum of the band is now shifted to 1660 cm^{-1} (Figure 3c). The shift to lower wavenumbers, when the dose increases from 100 kGy to 1 MGy could be attributed to additional C=N modes due to the formation of $R_2C=NH$ or $R_2C=NH^+$ species (Colthup et al., 1990).

The formation of C=C double bonds (or of terminal -CH_3 groups, for instance) in irradiated SBA-15-D is not observed on these infrared spectra, indicating that if these species are formed, their amount may be very low.

3.2.3. Proposed reaction mechanisms

Under ionizing radiation, the most striking feature arises from the H_2 production. As most of the sample consists in the silica matrix (see Figure S3a; the grafting represents 11.6% of the mass of SBA-15-D), irradiation of the SBA-15-D material mainly produces electron (e^-) and hole (h^+) within the material, according to Reaction 1:

SBA-15-D $\xrightarrow{ionizing\ radiation} e^- + h^+$ (R1)

These electron-hole pairs can recombine into excitons since the thickness of the SBA-15 walls is high enough (R2).

$e^- + h^+ \rightarrow {}^3\text{exciton}$ (R2)

The water molecules, if they are present within the SBA-15 material, are efficient trapping sites for these excitons, which leads to the cleavage of the OH bond and, consequently, to the formation of free radicals (R3) (Le Caër et al., 2005; Brodie-Linder et al., 2010).

$^3\text{exciton} + H_2O \rightarrow HO^{\bullet} + H^{\bullet}$ (R3)

The hydrogen atoms can then dimerize into dihydrogen according to (R4):

$H^{\bullet} + H^{\bullet} \rightarrow H_2$ (R4)

Irradiation will also affect SiOH bonds of silanol groups present in the material (R5):

$^3\text{exciton} + SiOH \rightarrow SiO^{\bullet} + H^{\bullet}$ (R5)

The grafted diamino ligand will also lead to the H_2 production. As shown above (Figure 3), this is mainly due to the cleavage of N-H bonds (as compared to C-H ones). The exciton transfer at the silica/organic part interface is at the origin of the selective cleavage of bonds (Zante et al., 2022).

$^3\text{exciton} + R_1R_2R_3NH \rightarrow R_1R_2R_3N^{\bullet} + H^{\bullet}$ (R6)

In this reaction, amine can be the secondary, the primary one or even the ammonium salt. As alkyl groups are electron donors, the electron density on the nitrogen atom is the lowest in ammonium salt; it then increases when going from primary amines to secondary ones. Therefore, the N-H bond is easier to break in secondary amines, then in primary amines, and, lastly in ammonium salts. This accounts for the observations that were made with the FT-IR experiments (Figure 3), which have suggested that the secondary amine functional group was the preferential attack site for ionizing radiation.

Of course, the exciton can also react with $-CH_2-$ groups leading to the formation of the hydrogen atom:

$^3\text{exciton} + R_1CH_2R_3 \rightarrow R_1{}^{\bullet}CHR_3 + H^{\bullet}$ (R7)

In this case, the FT-IR results suggest that the carbon mainly affected is adjacent to a nitrogen atom. Following (R6) or (R7), the formed hydrogen atom can abstract one hydrogen atom from -NH, leading to the release of H_2 and to the formation of a double C=N bond. The formed radicals can also, through a disproportionation reaction, lead to the formation of a C=N bond and to the formation of the initial species.

3.3. Impact of radiolysis on iodine capture

The goal was here to determine how the sorption capacity of grafted mesoporous silicas is affected if the sample is damaged due to previous irradiation. Note that we have verified that the ungrafted material (SBA-15) did not adsorb iodine. Iodine sorption experiments were performed on pristine material (SBA-15-D) and on this sample after irradiation at 1 MGy (SBA-15-D-1MGy) (Figure 4). The amount of iodine sorbed on the material was measured using UV-vis spectroscopy, by determining the residual concentration of diiodine in the cyclohexane solution (Falaise et al., 2013). Indeed, diiodine in cyclohexane is characterized by a maximum at 524 nm. From these measurements, the captured amount of iodine *Q*, expressed in mmol(I).g^{-1}, could be calculated. The maximum adsorption capacity of the non-irradiated material, corresponding to the pseudo-plateau obtained for the highest concentrations, is approximately 1.85 mmol(I).g^{-1} (= 23.5 wt%). This value is comparable to the sorption capacities measured on mesoporous-type materials synthesized for the same application (Massasso et al., 2015). TGA analysis of SBA15-D-I_2 indicated a greater final weight loss after treatment at 650°C, of approximately 45.5 wt% (Figure S3 in Supporting Information and Table 1). The TGA-MS experiments evidenced the release of iodine from 200°C (Ye et al., 2011), together with the release of H_2O, CO_2 and possibly NH_3 (Figure S3 in Supporting Information), which is consistent with the thermolysis of an amino-iodine complex. In comparison with the percentages of diamino and CO_2 determined from elemental analysis (17.1 wt%, see Table 1), it can be deduced that around 28.4 wt% of iodine (I) was sorbed. This value is comparable, although higher, to the value of 1.85 mmol(I).g^{-1} (23.5 wt%) determined from Figure 4. One explanation could be due to the fact that water is released at higher temperatures in presence of iodine than without, therefore leading to an overestimation of the % Δm from TGA experiments in Table 1.

When the material was previously irradiated at 1 MGy, then this sorption capacity is decreased to about 50%, with an adsorption capacity about 0.9 mmol(I).g^{-1} (= 11.4 wt%) (Figure 4). This decrease in iodine sorption in the case of the irradiated material may seem surprising at first glance. Indeed, imine functional groups, formed in the irradiated material as

proposed previously, are expected to be still able to capture diiodine, due to the presence of the lone pair on the nitrogen atom (Li et al., 2018; Chen et al., 2021). Indeed, the lone pair on the nitrogen atom behaves as a Lewis base, which has a strong affinity for the Lewis acidic diiodine. Therefore, another reason has to be invoked to account for such a decrease. A loss of amine groups on the surface of silica, due to irradiation, and not detected by our gas chromatography techniques, could explain this decrease in diiodine capture efficiency. Indeed, the comparison between the percentages of diamino in SBA-15-D-I_2 (10.5 wt%) and SBA-15-D-1MGy-I_2 (9.0 wt%) (Table 1) shows that the percentage of diamino has decreased upon irradiation. The H_2 and CO_2 production shown above cannot account for such a discrepancy between the diamino percentages. These results suggest that some amines or ammonia are produced upon irradiation, whose formation is difficult to follow with our experimental set-ups.

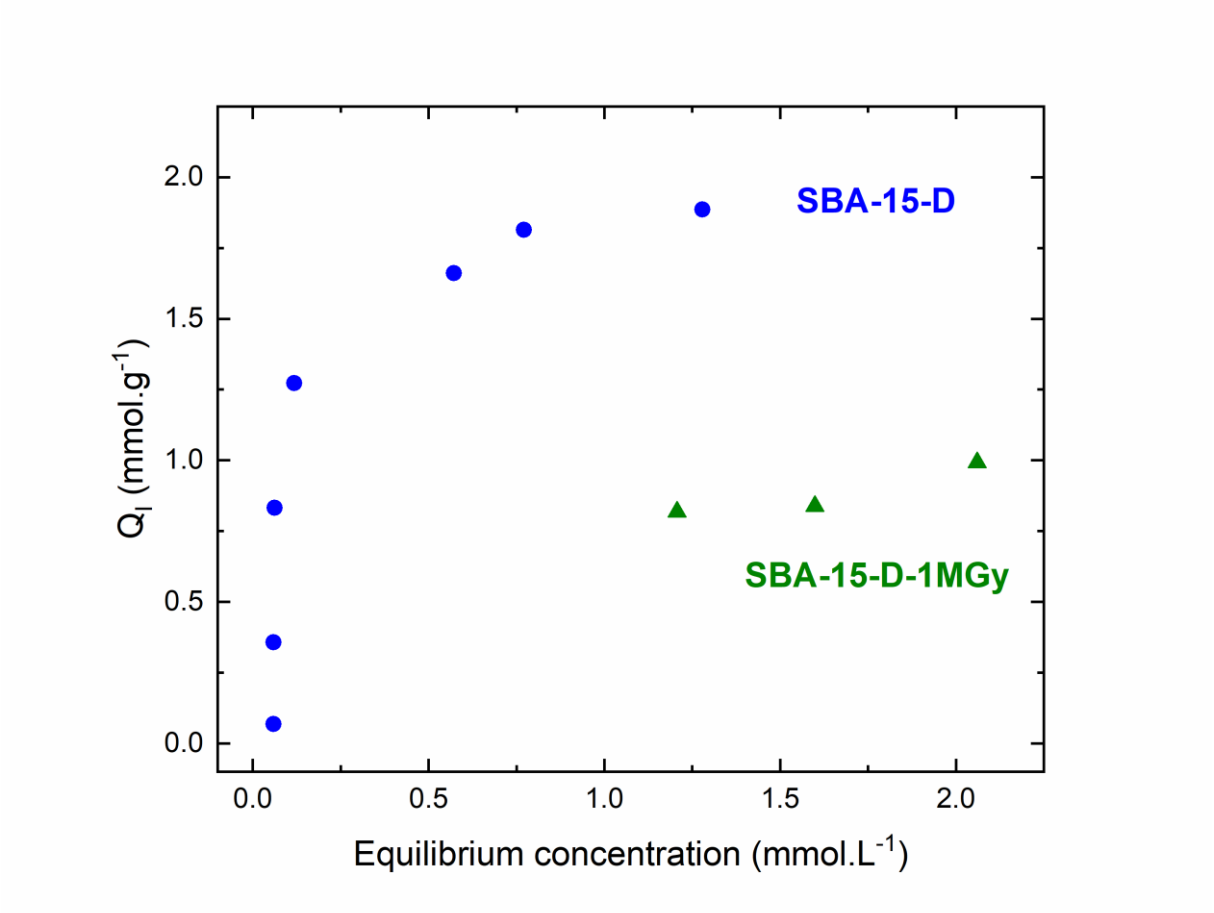

Figure 4. *Iodine (I) sorption isotherm in a cyclohexane solution for SBA-15-D (blue circles), and SBA-15-D-1MGy (green triangles) samples.*

Another way of investigating the fate of materials having sorbed I_2 involves irradiating them, and examining the behavior of diiodine after irradiation, as was carried for SBA-15-D-I_2 after irradiation at two doses: 500 kGy and 2.5 MGy. Indeed, a dose of the order of 1 MGy is representative of the dose that ^{129}I-trapping silica would receive over long periods (several thousands of years) at a content of 1 mmol.g^{-1}. Materials of the same type which would incorporate a comparable content of ^{131}I would receive a considerably higher dose (of the order of GGy in a few months). This latter dose is not available with our linear accelerator. Raman spectroscopy, in contrast to infrared spectroscopy, is a very well suited tool to investigate diiodine (Figure 5) (Hijazi et al., 2019). As expected, no bands were detected in the SBA-15-D sample in the 80-220 cm^{-1} spectral range (data not shown). In contrast, three bands were observed in this range for the SBA-15-D-I_2 sample. The band whose maximum is located at 109 cm^{-1} corresponds to the symmetric stretching of I_3^- (Svensson,Kloo, 2003; Pei et al., 2014; Hijazi et al., 2019). The presence of the I_3^- ion is also confirmed by the brown color of the powder upon iodine adsorption. Notably, the triiodide anion is formed through the strong charge transfer occurring between two I_2 molecules and the σ-electron donor diamine functional groups (Massasso et al., 2015). The broad band whose maximum shifts from 145 to 149 cm^{-1} when going from the pristine to irradiated samples, is assigned to the asymmetric stretching of I_3^-(Deplano et al., 1992; Massasso et al., 2015). Noteworthily, I_2 stretching modes can also contribute to this band (Mulazzi et al., 1981). The third band whose maximum is located around 200 cm^{-1} can be attributed to physisorbed I_2 (Svensson,Kloo, 2003; Massasso et al., 2015). This band is only observed in the spectra of irradiated samples.

The spectra displayed in Figure 5 are not quantitative. They were therefore normalized with respect to the most intense band whose maximum is at 109 cm^{-1}. The shift of the band around 150 cm^{-1} towards higher wavenumbers in irradiated samples, as well as the increase of its intensity with respect to the band at 109 cm^{-1}, suggests the formation of I_2. Lastly, physisorbed iodine is detected around 200 cm^{-1} in irradiated samples only. This evolution is consistent with a loss of iodine capture capacity upon irradiation. As suggested above, the release of amine functional groups could account for such a trend. Moreover, in irradiated samples, trapped iodine is more in the form of I_2 than of I_3^- as compared to the pristine material, with the presence of physisorbed I_2, i.e. weakly sorbed I_2.

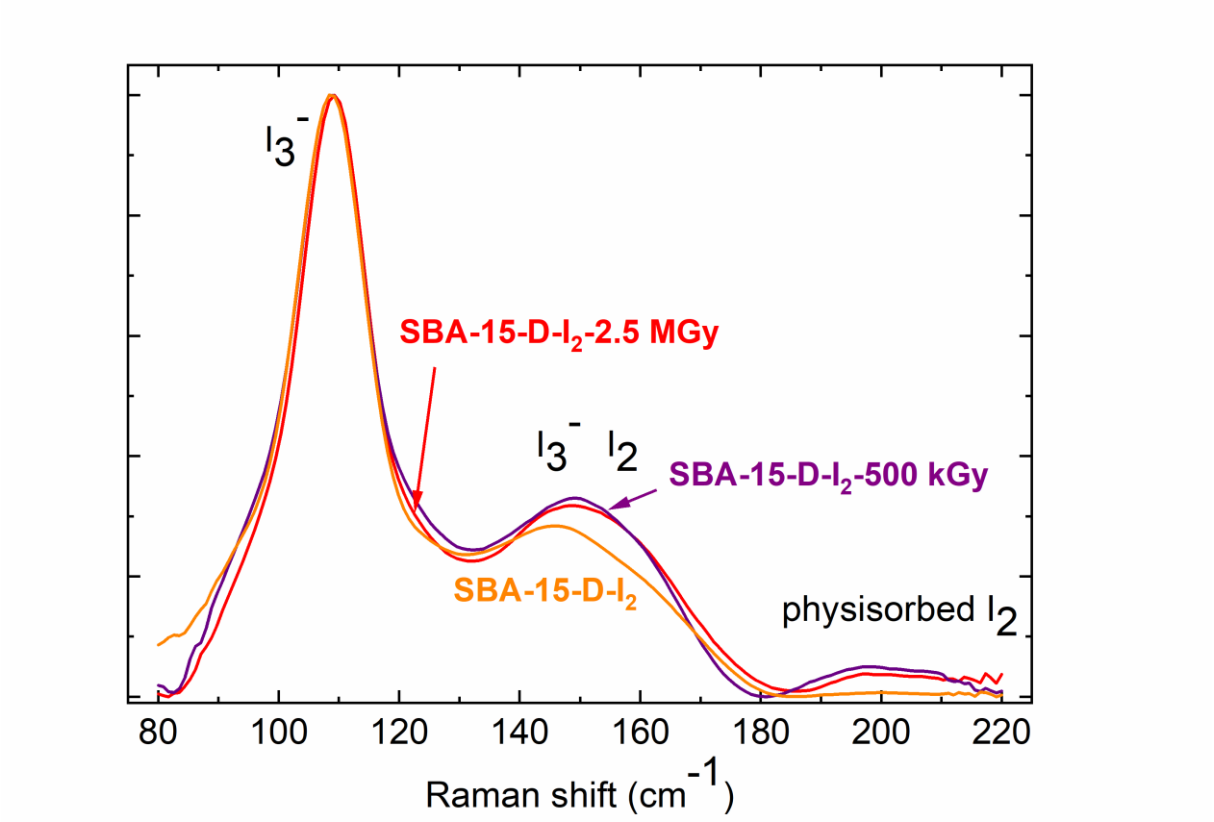

Figure 5. *Raman spectra of SBA-15-D-I_2 (orange) and of SBA-15-D-I_2 after irradiation at 500 kGy (purple) and at 2.5 MGy (red). As the spectra are not quantitative, they were normalized with respect to the most intense band at 109 cm^{-1}. No signal was recorded in the case of SBA-15-D.*

4. Conclusion

In order to capture iodine, grafted silica was synthesized. It benefited from the high surface area of the mesoporous silica SBA-15, together with the grafting with the N-[3-(trimethoxysilyl)propyl]ethylenediamine "diamino" ligand. This sample was shown to capture iodine, with a sorption capacity of around 0.23 g per gram of material. This material was also submitted to ionizing radiation in order to assess how its sorption capacity was affected by irradiation. At the high dose of 1 MGy, it was decreased by around 50%. At this dose, amines were certainly produced, leading to a decrease of the iodine sorption capacity which remained though significant. However, the modifications detected by the ligand were N-H and C-H bond cleavages, the first ones being preferred over the last ones, leading to the formation of imine C=N functional groups. This latter functional group is still expected to capture iodine thanks to the lone pairs of nitrogen atoms. The material having sorbed iodine was also irradiated at 0.5 and 2.5 MGy. In this case, the formation of physisorbed I_2 was detected in the irradiated samples, indicating the presence of less strongly sorbed iodine upon irradiation.

All these results prove that this mesoporous grafted silica is interesting as it captures iodine and can still work under harsh conditions such as the radiation emitted by radioactive iodine (^{129}I) up to a dose of the order of 1 MGy. Other parameters of interest would be to determine whether temperature and humidity affect the capture of iodine.

Acknowledgments

Funding from the Agence Nationale de la Recherche (ANR Automact N° ANR-18-CE05-0016-03) is gratefully acknowledged. The French EMIR&A network and Jorge Vieira are gratefully acknowledged for providing irradiation beam time at ALIENOR platform.

References

Brodie-Linder, N., Le Caër, S., Alam, M. S., Renault, J. P., Alba-Simionesco, C., 2010. H_2 Formation by Electron Irradiation of SBA-15 Materials and the Effect of Cu^{II} Grafting. Phys. Chem. Chem. Phys. 12 14188-14195.

Cambedouzou, J., Diat, O., 2012. Quantitative small-angle scattering on mesoporous silica powders: from morphological features to specific surface estimation. J. Appl. Cryst. 45 662-673.

Chapman, K. W., Chupas, P. J., Nenoff, T. M., 2010. Radioactive Iodine Capture in Silver-Containing Mordenites through Nanoscale Silver Iodide Formation. J. Am. Chem. Soc. 132 (26), 8897-8899.

Chen, P., He, X., Pang, M., Dong, X., Zhao, S., Zhang, W., 2020. Iodine Capture Using Zr-Based Metal–Organic Frameworks (Zr-MOFs): Adsorption Performance and Mechanism. ACS Appl. Mater. Interfaces 12 (18), 20429-20439.

Chen, R., Hu, T., Li, Y., 2021. Stable nitrogen-containing covalent organic framework as porous adsorbent for effective iodine capture from water. Reactive and Functional Polymers 159 104806.

Chen, Y., Sun, H., Yang, R., Wang, T., Pei, C., Xiang, Z., Zhu, Z., Liang, W., Li, A., Deng, W., 2015. Synthesis of conjugated microporous polymer nanotubes with large surface areas as absorbents for iodine and CO_2 uptake. J. Mater. Chem. A 3 (1), 87-91.

Colthup, N. B., Daly, L. H., Wiberley, S. E., 1990. Introduction to Infrared and Raman Spectroscopy, Third Edition. San Diego, Academic Press.

Deplano, P., Devillanova, F. A., Ferraro, J. R., Isaia, F., Lippolis, V., Mercuri, M. L., 1992. On the Use of Raman Spectroscopy in the Characterization of Iodine in Charge-Transfer Complexes. Appl. Spectroscopy 46 (11), 1625-1629.

Dhiman, S. B., LaVerne, J. A., 2013. Radiolysis of simple quaternary ammonium salt components of Amberlite resin. J. Nucl. Mat. 436 (1), 8-13.

Falaise, C., Volkringer, C., Facqueur, J., Bousquet, T., Gasnot, L., Loiseau, T., 2013. Capture of iodine in highly stable metal–organic frameworks: a systematic study. Chem. Comm. 49 (87), 10320-10322.

Fricke, H., Hart, E. J., 1966. Chemical Dosimetry in Radiation Dosimetry. F. H. Attix and W. C. Roesch. New York and London, Academic press. 2**:** 167-232.

García-Toraño, E., Altzitzoglou, T., Auerbach, P., Bé, M.-M., Bobin, C., Cassette, P., Chartier, F., Dersch, R., Fernández, M., Isnard, H., Kossert, K., Lourenço, V., Nähle, O., Nonell, A., Peyrés, V., Pommé, S., Rozkov, A., Sánchez-Cabezudo, A., Sochorová, J., 2018. The half-life of 129I. App. Radiat. Isotopes 140 157-162.
Golub, A. A., Zubenko, A. I., Zhmud, B. V., 1996. γ-APTES Modified Silica Gels: The Structure of the Surface Layer. Journal of Colloid and Interface Science 179 (2), 482-487.
Hijazi, A., Azambre, B., Finqueneisel, G., Vibert, F., Blin, J. L., 2019. High iodine adsorption by polyethyleneimine impregnated nanosilica sorbents. Microporous Mesoporous Mat. 288 109586.
Hou, X., Hansen, V., Aldahan, A., Possnert, G., Lind, O. C., Lujaniene, G., 2009. A review on speciation of iodine-129 in the environmental and biological samples. Analytica Chimica Acta 632 (2), 181-196.
Huve, J., Ryzhikov, A., Nouali, H., Lalia, V., Augé, G., Daou, T. J., 2018. Porous sorbents for the capture of radioactive iodine compounds: a review. RSC Adv. 8 (51), 29248-29273.
Kataoka, H., 1996. Derivatization reactions for the determination of amines by gas chromatography and their applications in environmental analysis. J. Chromatography A 733 (1), 19-34.
Lago, D. C., Sánchez, A. D., Prado, M. O., 2022. Cesium immobilization in porous silica and 137Cs self-heating simulations. J. Nucl. Mat. 565, 153697.
Le Caër, S., Rotureau, P., Brunet, F., Charpentier, T., Blain, G., Renault, J. P., Mialocq, J.-C., 2005. Radiolysis of Confined Water: Hydrogen Production at a High Dose Rate. ChemPhysChem 6, 2585-2596.
Li, Y., Chen, W., Hao, W., Li, Y., Chen, L., 2018. Covalent Organic Frameworks Constructed from Flexible Building Blocks with High Adsorption Capacity for Pollutants. ACS Appl. Nano Mater. 1 (9), 4756-4761.
Lin, J., Toquer, G., Grygiel, C., Dourdain, S., Guari, Y., Rey, C., Causse, J., Deschanels, X., 2021. Behavior of mesoporous silica under 2 MeV electron beam irradiation. Microporous Mesoporous Mater. 328, 111454.
Lou, Y., Toquer, G., Dourdain, S., Rey, C., Grygiel, C., Simeone, D., Deschanels, X., 2015. Structure evolution of mesoporous silica SBA-15 and MCM-41 under swift heavy ion irradiation. Nucl. Instrum. Meth. Phys. Res. B 365, 336-341.
Lou, Y., Dourdain, S., Rey, C., Serruys, Y., Simeone, D., Mollard, N., Deschanels, X., 2017. Structure evolution of mesoporous silica under heavy ion irradiations of intermediate energies. Microporous Mesoporous Mater. 251, 146-154.
Maddrell, E. R., Vance, E. R., Gregg, D. J., 2015. Capture of iodine from the vapour phase and immobilisation as sodalite. J. Nucl. Mat. 467 271-279.
Makowski, P., Deschanels, X., Grandjean, A., Meyer, D., Toquer, G., Goettmann, F., 2012. Mesoporous materials in the field of nuclear industry: applications and perspectives. New J. Chem. 36 (3), 531-541.
Maria Chong, A. S., Zhao, X. S., 2003. Functionalization of SBA-15 with APTES and Characterization of Functionalized Materials. J. Phys. Chem. B 107 (46), 12650-12657.
Massasso, G., Long, J., Guerin, C., Grandjean, A., Onida, B., Guari, Y., Larionova, J., Maurin, G., Devautour-Vinot, S., 2015. Understanding the Host/Guest Interactions in Iodine/Hofmann-Type Clathrate Ni(pz)[Ni(CN)4] System. J. Phys. Chem. C 119 (17), 9395-9401.
Massasso, G., Rodriguez-Castillo, M., Long, J., Grandjean, A., Onida, B., Guari, Y., Guerin, C., Larionova, J., 2015. Nanocomposites based on Hofmann-type structure NiII(pz)[NiII(CN)4] (pz = pyrazine) nanoparticles for reversible iodine capture. J. Mater. Chem. A 3 (1), 179-188.

Massasso, G., Rodríguez-Castillo, M., Long, J., Haines, J., Devautour-Vinot, S., Maurin, G., Grandjean, A., Onida, B., Donnadieu, B., Larionova, J., Guérin, C., Guari, Y., 2015. Molecular iodine adsorption within Hofmann-type structures $M(L)[M'(CN)_4]$ (M = Ni, Co; M′ = Ni, Pd, Pt): impact of their composition. Dalton Trans. 44 (44), 19357-19369.
Meléndez-Ortiz, H. I., Perera-Mercado, Y., Mercado-Silva, J. A., Olivares-Maldonado, Y., Castruita, G., García-Cerda, L. A., 2014. Functionalization with amine-containing organosilane of mesoporous silica MCM-41 and MCM-48 obtained at room temperature. Ceramics International 40 (7, Part A), 9701-9707.
Mnasri, N., Charnay, C., de Ménorval, L.-C., Moussaoui, Y., Elaloui, E., Zajac, J., 2014. Silver nanoparticle-containing submicron-in-size mesoporous silica-based systems for iodine entrapment and immobilization from gas phase. Microporous Mesoporous Mat. 196 305-313.
Mulazzi, E., Pollini, I., Piseri, L., Tubino, R., 1981. Selective resonant Raman enhancement in polyiodide chains. Phys. Rev. B 24 (6), 3555-3563.
Nandanwar, S. U., Coldsnow, K., Green, M., Utgikar, V., Sabharwall, P., Aston, D. E., 2016. Activity of nanostructured C@ETS-10 sorbent for capture of volatile radioactive iodine from gas stream. Chem. Eng. J. 287 593-601.
Pei, C., Ben, T., Xu, S., Qiu, S., 2014. Ultrahigh iodine adsorption in porous organic frameworks. J. Mater. Chem. A 2 (20), 7179-7187.
Qian, X., Zhu, Z.-Q., Sun, H.-X., Ren, F., Mu, P., Liang, W., Chen, L., Li, A., 2016. Capture and Reversible Storage of Volatile Iodine by Novel Conjugated Microporous Polymers Containing Thiophene Units. ACS Appl. Mater. Interfaces 8 (32), 21063-21069.
Riley, B. J., Vienna, J. D., Strachan, D. M., McCloy, J. S., Jerden, J. L., 2016. Materials and processes for the effective capture and immobilization of radioiodine: A review. J. Nucl. Mat. 470 307-326.
Sanchez-Vicente, Y., Stevens, L., Pando, C., Cabanas, A., 2020. Functionalization of Silica SBA-15 with [3-(2-Aminoethylamino)Propyl] Trimethoxysilane in Supercritical CO2 Modified with Methanol or Ethanol for Carbon Capture. Energies 13 (21), 5804.
Sangvanich, T., Sukwarotwat, V., Wiacek, R. J., Grudzien, R. M., Fryxell, G. E., Addleman, R. S., Timchalk, C., Yantasee, W., 2010. Selective capture of cesium and thallium from natural waters and simulated wastes with copper ferrocyanide functionalized mesoporous silica. J. Hazard. Mater. 182 (1), 225-231.
Sava Gallis, D. F., Ermanoski, I., Greathouse, J. A., Chapman, K. W., Nenoff, T. M., 2017. Iodine Gas Adsorption in Nanoporous Materials: A Combined Experiment–Modeling Study. Ind. Eng. Chem. Res. 56 (8), 2331-2338.
Serna-Guerrero, R., Belmabkhout, Y., Sayari, A., 2010. Modeling CO_2 adsorption on amine-functionalized mesoporous silica: 1. A semi-empirical equilibrium model. Chem. Eng. J. 161 (1), 173-181.
Simpson, M. F., 2013. Nuclear Fuel Reprocessing Technologies and Commercialization. Sci. Technol. Nucl. Installations 2013 815693.
Spinks, J. W. T., Woods, R. J., 1990. An Introduction to Radiation Chemistry. New York, USA, Wiley-Interscience Publication.
Svensson, P. H., Kloo, L., 2003. Synthesis, Structure, and Bonding in Polyiodide and Metal Iodide−Iodine Systems. Chem. Rev. 103 (5), 1649-1684.
Tang, Y., Huang, H., Li, J., Xue, W., Zhong, C., 2019. IL-induced formation of dynamic complex iodide anions in IL@MOF composites for efficient iodine capture. J. Mater. Chem. A 7 (31), 18324-18329.
Valizadeh, B., Nguyen, T. N., Smit, B., Stylianou, K. C., 2018. Porous Metal–Organic Framework@Polymer Beads for Iodine Capture and Recovery Using a Gas-Sparged Column. Adv. Funct. Mater. 28 (30), 1801596.

Yang, J. H., Cho, Y.-J., Shin, J. M., Yim, M.-S., 2015. Bismuth-embedded SBA-15 mesoporous silica for radioactive iodine capture and stable storage. J. Nucl. Mat. 465 556-564.
Ye, J. T., Iwasa, Y., Tang, Z. K., 2011. Thermal variations of iodine nanostructures inside the channels of $AlPO_4$-5 zeolite single crystals. Phys. Rev. B 83 (19), 193409.
Zante, G., Bouniol, V., Sene, S., Rey, C., Causse, J., Larionova, J., Guari, Y., Deschanels, X., Le Caër, S., 2022. Grafted mesoporous silicas for radionuclide uptake: Radiolytic stability under electron irradiation. Microporous Mesoporous Mater. 336 111851.
Zhao, D., Feng, J., Huo, Q., Melosh, N., Fredrickson, G. H., Chmelka, B. F., Stucky, G. D., 1998. Triblock Copolymer Syntheses of Mesoporous Silica with Periodic 50 to 300 Angstrom Pores. Science 279 (5350), 548-552.
Zhu, Y., Ji, Y.-J., Wang, D.-G., Zhang, Y., Tang, H., Jia, X.-R., Song, M., Yu, G., Kuang, G.-C., 2017. BODIPY-based conjugated porous polymers for highly efficient volatile iodine capture. J. Mater. Chem. A 5 (14), 6622-6629.
Zhuravlev, L. T., 2000. The surface chemistry of amorphous silica. Zhuravlev model. Colloids and Surfaces A 173 (1), 1-38.

Graphical abstract

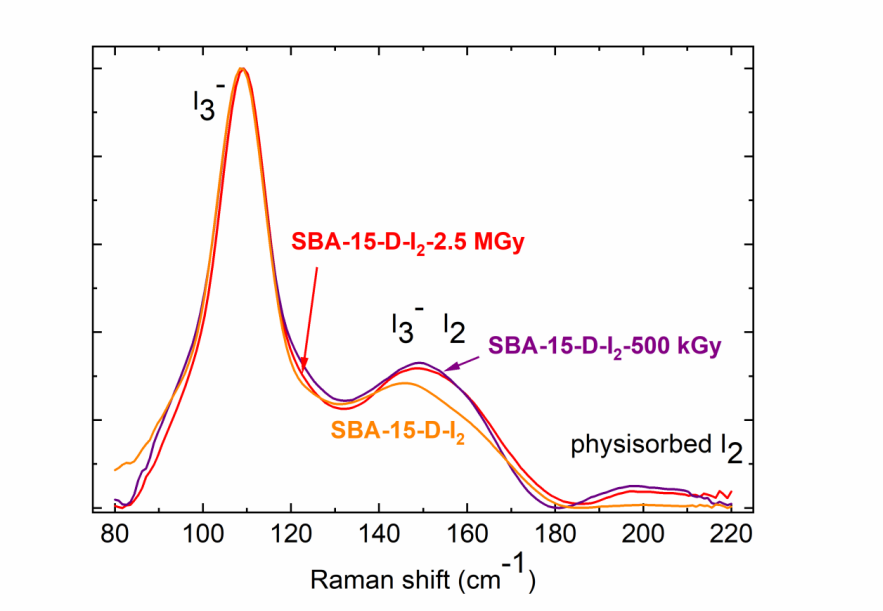

The behavior of grafted mesoporous silica having sorbed iodine was followed upon irradiation.